ChemPubSoc Europe

DOI: 10.1002/cphc.201900813

CHEMPHYSCHEM Communications

# Threshold Photoelectron Spectroscopy of IO and HOI

Domenik Schleier,[a] Engelbert Reusch,[a] Lisa Lummel,[a] Patrick Hemberger,[b] and Ingo Fischer*[a]

Iodine oxides appear as reactive intermediates in atmospheric chemistry. Here, we investigate IO and HOI by mass-selective threshold photoelectron spectroscopy (ms-TPES), using synchrotron radiation. IO and HOI are generated by photolyzing iodine in the presence of ozone. For both molecules, accurate ionization energies are determined, $9.71 \pm 0.02$ eV for IO and $9.79 \pm 0.02$ eV for HOI. The strong spin-spin interaction in the $^3\Sigma^-$ ground state of $IO^+$ leads to an energy splitting into the $\Omega = 0$ and $\Omega = \pm 1$ sublevels. Upon ionization, the I–O bond shortens significantly in both molecules; thus, a vibrational progression, assigned to the I–O stretch, is apparent in both spectra.

Atmospheric iodine is linked to the catalytic destruction of ozone by formation of iodine oxide particles (IOPs), which influence the oxidative capacities of the atmosphere.[1] IOPs can act as cloud condensation nuclei (CCN), therefore influencing cloud lifetimes and also make a negative contribution to the radiative flux in the tropical troposphere.[2] Numerous studies focused on the formation of IOPs and their influence on atmospheric processes.[3] The key species for this process have been identified to be IO and HOI,[4] which can be formed by reaction (1) and (2), respectively:

$$I + O_3 \rightarrow IO + O_2 \quad (1)$$

$$I_2 + OH \rightarrow HOI + I \quad (2)$$

Further self-reactions of IO molecules generates the dimer $(IO)_2$ as well as OIO, which both can react further to form larger IOPs. However, until now spectroscopic knowledge on the iodine oxides is limited. Key intermediates like IO and HOI have been spectroscopically characterized by UV/Vis,[5] IR,[6] EPR,[7] and microwave spectroscopy[8] as well as photoelectron detachment.[9] However, thermodynamic information as well as information on their cations is still scarce. Photoionization time-of-flight mass spectrometry (PI-TOF-MS) has just recently been employed to investigate the nucleation process of IOPs.[10] For ionization-based detection schemes in kinetic studies, knowledge of the ionization energies (IE) is a prerequisite. The relativistic effects that play an increasingly important role in molecules containing heavy elements like iodine, complicate spectral assignments. A first report on the photoionization of IO determined the IE of the IO radical using photoionization efficiency (PIE) curves to be $9.74 \pm 0.02$ eV.[11] A second step at 9.86 eV in the PIE curve was assigned to a vibrational overtone. However, the determination of accurate IE's and vibrational frequencies based on PIE curves is associated with large error bars. In fact Hassanzadeh *et al.* questioned this assignment based on theory.[12] Their high-level relativistic calculations yielded a pronounced spin-spin-splitting in $IO^+$, leading them to assign the two steps to the $\Omega = 0$ and $\Omega = \pm 1$ levels of the $X^+\ ^3\Sigma^-$ ground state of the cation. Also for HOI only low resolution PIE curves have been reported.[10b,13] In order to assess the previous assignment experimentally, we reinvestigated the photoionization of IO and HOI by photoelectron-photoion coincidence (PEPICO) spectroscopy using tunable Vacuum Ultraviolet (VUV) synchrotron radiation.[14] Detecting electrons and ions in coincidence permits to record photoion mass-selected threshold-photoelectron spectra (ms-TPES) of reactive molecules[14b,15] and to distinguish isomers, even when the differences in the IE are small[16] or when a large number of species is present.[17] Combined with synchrotron radiation, PEPICO has been established as an analytical tool to monitor gas-phase kinetics,[18] combustion reactions[19] and catalysis.[20]

## Results and Discussion

Iodine atoms were generated by photolyzing $I_2$ at 532 nm in a flow reactor resulting in two iodine atoms in two different spin-orbit states according to reaction (3).[3f,21]

$$I_2 + h\nu\ (532\,nm) \rightarrow I\ (^2P_{3/2}) + I\ (^2P_{1/2}) \quad (3)$$

Subsequent collision with the bath gas quenches spin-orbit excited iodine atoms ($^2P_{1/2}$) and subsequent reaction with $O_3$ forms IO, according to reaction (1a).

$$I\ (^2P_{3/2}) + O_3 \rightarrow IO + O_2 \quad (1a)$$

[a] D. Schleier, E. Reusch, L. Lummel, Prof. Dr. I. Fischer
Institute for Physical and Theoretical Chemistry
University of Würzburg
Am Hubland
97074 Würzburg, Germany
E-mail: ingo.fischer@uni-wuerzburg.de
[b] Dr. P. Hemberger
Laboratory for Femtochemistry and Synchrotron Radiation
Paul Scherrer Institute (PSI)
5232 Villigen, Switzerland
E-mail: patrick.hemberger@psi.ch

HOI on the other hand appeared as a side product in the reactor. Most likely formed via (2) due to reaction with OH originating from residual water impurities inside the reactor.

Figure 1 shows the time-of-flight mass spectrum recorded at 9.90 eV with the photolysis laser present. The most intense peak at *m/z* 254 arises from the precursor $I_2$, while the other peaks at *m/z* = 143 and 144 are assigned to IO and HOI respectively. Three distinct peaks marked with asterisks at 206, 208 and 213 are also visible and most likely due to contaminants from previous experiments. Up to 10.60 eV no masses of larger IO species have been detected. The use of higher photon energies was impeded by the transmission of the $MgF_2$ window. The IE of atomic iodine is 10.43 eV, however even at this energy no iodine atoms were detected. Obviously, the excess of ozone in the reactor quantitatively transforms iodine atoms into IO.

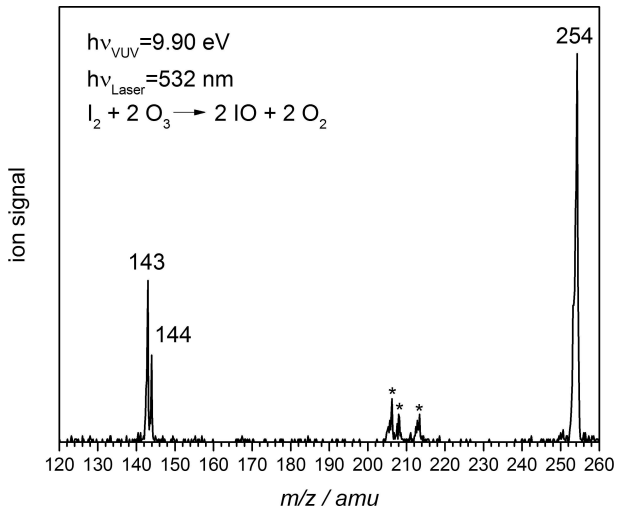


**Figure 1.** Mass spectrum of the $I_2$ and $O_3$ mixture recorded at 9.90 eV after photolysis at 532 nm. The peaks indicated with an asterisk are most likely impurities from previous experiments.

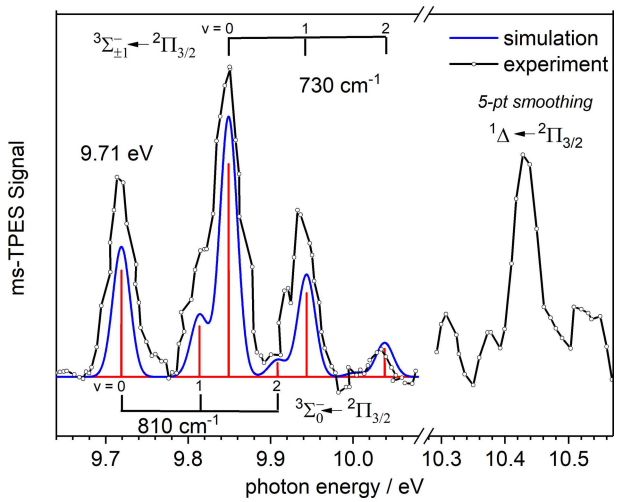


**Figure 2.** ms-TPES of the IO radical. Transitions into the $^3\Sigma^-$ and the excited $a^{+1}\Delta$ state of $IO^+$ are observed and the spin-spin splitting in the $X^{+3}\Sigma^-$ state can be resolved. The red sticks correspond to the FCF computed in Ref. [12]

**ms-TPES**

The ms-TPES of IO (m/z = 143), depicted in Figure 2 exhibits several distinct bands. The first peak at 9.71 ± 0.02 eV is assigned to the ionization energy and the origin of the $X^{+3}\Sigma^- \leftarrow X\ ^2\Pi_{3/2}$ transition. The error bars correspond to the full width at half maximum (fwhm) of the band. Computations yielded values of 9.59 eV (Gaussian 2 procedure)[11] and 9.60 eV (CCSD(T) level of theory).[12] Compared to BrO[22] the IE is lower by about 0.75 eV. As the bond length of IO changes upon ionization from 1.868 Å[23] to 1.824 Å[12] and because an electron is ejected from an antibonding orbital, a pronounced vibrational progression can be expected. The most intense band is observed at 9.85 eV and coincides with a step in the photoion yield. This step was assigned by Zhang *et al.* to the transition into the $v^+ = 1$ state of $IO^+$.[11] However, neither the vibrational energy of 0.14 eV (1130 $cm^{-1}$) nor the relative intensity are in agreement with the computations. Furthermore, no regular progression is formed with the third band at 9.94 eV. The CCSD(T)/6311 + G(3df) calculations of Hassanzadeh *et al.* suggest a different assignment, based on a pronounced spin-spin splitting in $IO^+$, which leads to a splitting of the triplet state into two energetically separated components, a lower energy $^3\Sigma^-_0$ and a degenerate higher energy $^3\Sigma^-_{\pm1}$ component. We therefore assign the band at 9.85 eV to the higher $X^{+3}\Sigma^-_{\pm1} \leftarrow X\ ^2\Pi_{3/2}$ transition. Consequently, the value of 0.14 eV (1130 $cm^{-1}$) corresponds to the spin-spin splitting in the $X^{+3}\Sigma^-$ state, in good agreement with the computed value for $2\lambda_e \approx 900\ cm^{-1}$, which slightly depended on the chosen method. The two bands at 9.95 eV and 10.04 eV are members of a vibrational progression with a wavenumber of 730 ± 40 $cm^{-1}$ and correspond to transitions into $v^+ = 1$ and $v^+ = 2$ of the $^3\Sigma^-_{\pm1}$ state. The value is in perfect agreement with the calculated one of 764 $cm^{-1}$.[12] The vibrational progression associated with the $X^{+3}\Sigma^-_0$ transition on the other hand is superimposed with the more intense transition into the $^3\Sigma^-_{\pm1}$ state and can only be observed as shoulders. The red sticks in Figure 2 represent Franck-Condon factors (FCF) taken from Ref. [12] and the simulation (blue line, 0 K) is in excellent agreement with the experimental spectrum. Note that a statistical ratio of 1:2 has been assumed in the calculations for the two spin components. A small sequence band transition might be visible on the low-energy side of the origin.

At higher photon energies a further band is visible in the spectrum, which is attributed to the transition into the lowest singlet state $a^{+1}\Delta \leftarrow X\ ^2\Pi_{3/2}$ at 10.43 ± 0.02 eV. This value compares well with the computed one at 10.45 eV.[12] However, the transition intensity is significantly lower. In the earlier PIE curves no significant rise of the ion signal could be observed at this photon energy.[11] The experimental results thus point at a smaller ionization cross section for the $a^{+1}\Delta$ state. No vibrational progression is visible in the $a^{+1}\Delta \leftarrow X\ ^2\Pi_{3/2}$ transition, in agreement with the computed dominance of the origin transition, due to the small change in geometry upon ionization. The signal/noise ratio in this part of the spectrum is low, because of the low photon flux at photon energies close to

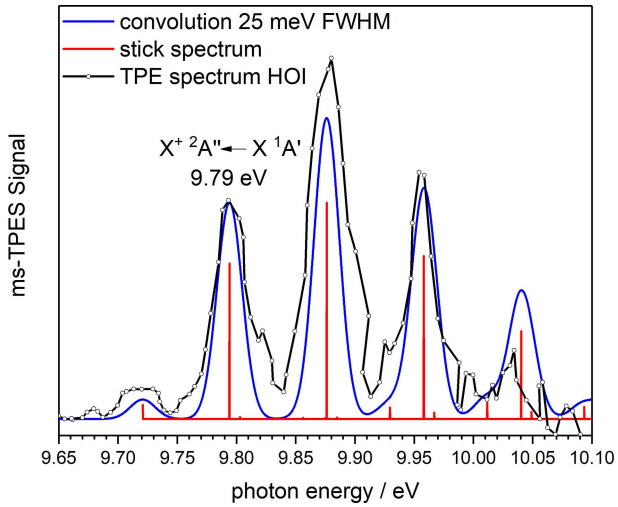


**Figure 3.** TPES of the HOI molecule. The ionization energy was determined to be 9.79 ± 0.02 eV. The vibrational progression originates from the I–O stretch mode.

the cutoff of the $MgF_2$ window. Weak transitions can therefore not be observed.

The TPES $X^{+2}A''\leftarrow X^1A'$ transition of HOI (m/z = 144) is presented in Figure 3. An ionization energy of 9.79 ± 0.02 eV is determined and a vibrational progression of around 660 $cm^{-1}$ is apparent. The values agree well with the IE = 9.81 eV and the vibrational progression at $\omega^+ = 702\ cm^{-1}$ extracted from a PIE curve by Monks *et al.*,[13] but is somewhat higher than the 9.70 eV, reported by Wei *et al.*[10b] Our DFT calculations yield values of 9.82 eV for the ionization energy and $\omega_3{}^+ = 665\ cm^{-1}$ for the I–O stretch mode $\nu_3{}^+$ in $HOI^+$. Upon ionization the I–O bond length shortens significantly from 2.014 Å to 1.920 Å while the O–H bond length increases slightly from 0.966 Å to 0.980 Å. The bond angle also increases from 105.1° in the neutral molecule to 111.0° in the cation. Very similar geometry parameters have been reported by Ma *et al.*,[11] who computed an IE of 9.74 eV. The vibrational progression is thus in line with the ejection of an electron from an I–O antibonding orbital, therefore exciting $\nu_3{}^+$ in $HOI^+$.[13] Using the calculated vibrational frequencies and geometries, the progression in the spectrum are simulated very well. Small shoulders in the intense bands are visible that can be assigned to the $\nu_2{}^+$ bending mode with $\omega_2{}^+ = 1070\ cm^{-1}$ and a series of combination bands $2^13^n$. The calculations predict a value of 1094 $cm^{-1}$ for $\omega_2{}^+$. A weak band at 9.72 eV is assigned to the $3_1{}^0$ hot band and is also well represented in the simulation, assuming a temperature of 298 K.

## Conclusion

IO and HOI, reactive molecules of atmospheric relevance, have been investigated using threshold photoelectron spectroscopy. To generate both molecules, iodine was photolyzed in a slow-flow reactor and subsequently reacted with ozone. The $X^{+3}\Sigma^-$ ground state of $IO^+$ is split into two components due to spin-spin interaction. For the IE of the $X^{+3}\Sigma^-_0\leftarrow X\ ^2\Pi_{3/2}$ transition a value of 9.71 ± 0.02 eV has been determined. The upper $^3\Sigma^-_{\pm1}$ state is 0.14 eV higher in energy. Since the I–O bond shortens significantly upon ionization, a vibrational progression has been observed with wavenumbers of 810 $cm^{-1}$ ($^3\Sigma^-_0$) and 730 $cm^{-1}$ ($^3\Sigma^-_{\pm1}$), which are greater than in the $X\ ^2\Pi_{3/2}$ neutral ground state (682 $cm^{-1}$).[23a] The experimental data are in excellent agreement with computations, which report a value of $2\lambda_e \approx 900\ cm^{-1}$ for the spin-spin splitting. Furthermore, the transition into the excited $a^+{}^1\Delta$ state is observed at 10.43 eV. HOI is presumably formed in a side reaction with water traces in the flow tube reactor. We determined an IE for HOI of 9.79 ± 0.02 eV and a wavenumber of 660 $cm^{-1}$ for the $\nu_3{}^+$ I–O stretching mode. In both molecules, an electron is removed from an I–O antibonding orbital and therefore the bond order increases in the cations. Our data agree qualitatively with those obtained from previous photoion efficiency curves, but offer a much higher accuracy.

## Methods

Experiments were performed at the VUV beamline of the Swiss Light Source (SLS), using the double imaging CRF-PEPICO spectrometer.[24] IO and HOI were generated in a side-sampled 1.25 cm (1/2″) O.D. quartz tube photolysis flow reactor, coated with halocarbon wax and mounted parallel to the synchrotron beam. The iodine vapor was introduced into the flow tube by flowing argon through a glass container filled with solid $I_2$. The flow was regulated by a valve at the front of the reactor to optimize the IO signal. Ozone was produced by a commercially available ozone generator (Fischer 502/10) through a silent electric discharge of $O_2$, producing a mixture of about 5% $O_3$ in $O_2$, which was introduced as a metered flow into the reactor. The pressure inside the reactor was kept at 0.6 mbar,[24] the $O_3$ concentration was around $7\cdot10^{14}$ molecules $cm^{-3}$. The total gas flow rate was set high enough to completely replace the gas mixture in the reactor tube with a fresh sample in-between two consecutive laser pulses in order to avoid accumulation of reaction products. The 2nd harmonic of a 10 Hz Nd:YAG laser (Quantel, Q-smart 850) at around 190 mJ/$cm^2$ was employed for photolysis. The laser beam propagated down the reactor and illuminated the full volume of the reactor tube. At the halfway point of the tube the mixture effused through a 300 μm hole in the wall into the experimental chamber. The signal was integrated over the complete cycle between photolysis pulses. The pressure in the ionization chamber was kept below $7\times10^{-6}$ mbar. The effusive gas beam was crossed by the VUV radiation at a distance of 21 ± 4 mm away from the flow tube. A constant extraction field of 250 V $cm^{-1}$ accelerated the generated photoions and photoelectrons in opposite directions towards the Roentdek DLD40 position-sensitive delay-line detectors. In this setup, the electron-hit times provide a start signal for the ion time-of-flight mass analysis in a multiple-start/multiple-stop data acquisition scheme.[25] The photon energy was calibrated using the Ar 11 s′–14 s′ autoionization resonances in the first and second order of the monochromator grating (150 l/mm). Ionization energies are corrected for the Stark-shift by the extraction field (≈60–70 $cm^{-1}$). The VUV photon energy was scanned between 9.65–10.30 eV to record a TPES of the $^3\Sigma^-_0\leftarrow{}^2\Pi_{3/2}$ and $^3\Sigma^-_{\pm1}\leftarrow{}^2\Pi_{3/2}$ transitions in IO as well as the ms-TPES of HOI and from 10.30–10.60 eV for the $^1\Delta\leftarrow{}^2\Pi_{3/2}$ transition. Higher harmonic radiation was suppressed by a $MgF_2$ window. Threshold electrons were selected with an energy

resolution of 5 meV for the energy range up to 10.30 eV and 10 meV for the energy range from 10.30–10.60 eV. The contribution of hot electrons was subtracted, following a procedure similar to the one given in Ref. [26], and each spectrum was normalized to the photon flux. Quantum chemical calculations on HOI were performed with the Gaussian 09 suite of programs.[27] In all calculations the B3LYP density functional was used. For iodine the correlation consistent polarized triple-ζ-PP basis set (aug-cc-pVTZ-PP)[23b] was employed, including a relativistic pseudopotential for the inner shell electrons (1s–3d). For all other elements the aug-cc-pVTZ basis set was utilized. Initially the molecular geometries were optimized and subsequently the vibrational wavenumbers and force constants of the neutral and the cation were computed at this geometry. The photoelectron spectra were simulated using the program eZSpectrum.[28]

## Acknowledgements

*Financial support by the Deutsche Forschungsgemeinschaft, research training group GRK 2112 and FI575/13-1 is acknowledged. The experiments were conducted at the VUV beamline of the Swiss Light Source storage ring, Paul Scherrer Institute (PSI). We are also grateful for the financial support by the Swiss Federal Office for Energy (BFE Contract Number SI/501269-01) and for the technical support by Patrick Ascher.*

## Conflict of Interest

The authors declare no conflict of interest.

**Keywords:** ionization potential · radicals · reactive intermediates · photolysis · synchrotron radiation

[1] a) B. Alicke, K. Hebestreit, J. Stutz, U. Platt, *Nature* **1999**, *397*, 572–573; b) G. McFiggans, J. M. C. Plane, B. J. Allan, L. J. Carpenter, H. Coe, C. O'Dowd, *J Geophys. Res. Atmos.* **2000**, *105*, 14371–14385.

[2] A. Saiz-Lopez, J. M. C. Plane, A. R. Baker, L. J. Carpenter, R. von Glasow, J. C. Gómez Martín, G. McFiggans, R. W. Saunders, *Chem. Rev.* **2012**, *112*, 1773–1804.

[3] a) T. Sherwen, M. J. Evans, L. J. Carpenter, S. J. Andrews, R. T. Lidster, B. Dix, T. K. Koenig, R. Sinreich, I. Ortega, R. Volkamer, A. Saiz-Lopez, C. Prados-Roman, A. S. Mahajan, C. Ordóñez, *Atmos. Chem. Phys.* **2016**, *16*, 1161–1186; b) C. R. Thompson, P. B. Shepson, J. Liao, L. G. Huey, E. C. Apel, C. A. Cantrell, F. Flocke, J. Orlando, A. Fried, S. R. Hall, R. S. Hornbrook, D. J. Knapp, R. L. Mauldin Iii, D. D. Montzka, B. C. Sive, K. Ullmann, P. Weibring, A. Weinheimer, *Atmos. Chem. Phys.* **2015**, *15*, 9651–9679; c) B. Laszlo, M. J. Kurylo, R. E. Huie, *J. Phys. Chem.* **1995**, *99*, 11701–11707; d) M. E. Jenkin, R. A. Cox, *J. Phys. Chem.* **1985**, *89*, 192–199; e) A. Vipond, C. E. Canosa-Mas, M. L. Flugge, D. J. Gray, D. E. Shallcross, D. Shah, R. P. Wayne, *Phys. Chem. Chem. Phys.* **2002**, *4*, 3648–3658; f) M. E. Tucceri, T. J. Dillon, J. N. Crowley, *Phys. Chem. Chem. Phys.* **2005**, *7*, 1657–1663.

[4] C. D. O'Dowd, J. L. Jimenez, R. Bahreini, R. C. Flagan, J. H. Seinfeld, K. Hämeri, L. Pirjola, M. Kulmala, S. G. Jennings, T. Hoffmann, *Nature* **2002**, *417*, 632–636.

[5] R. A. Durie, D. A. Ramsay, *Can. J. Phys.* **1958**, *36*, 35–53.

[6] a) I. Barnes, K. H. Becker, J. Starcke, *Chem. Phys. Lett.* **1992**, *196*, 578–582; b) N. Walker, D. E. Tevault, R. R. Smardzewski, *J. Chem. Phys.* **1978**, *69*, 564–568.

[7] J. M. Brown, C. R. Byfleet, B. J. Howard, D. K. Russell, *Mol. Phys.* **1972**, *23*, 457–468.

[8] a) H. Ozeki, S. Saito, *J. Chem. Phys.* **2004**, *120*, 5110–5116; b) S. Saito, *J. Mol. Spectrosc.* **1973**, *48*, 530–535.

[9] M. K. Gilles, M. L. Polak, W. C. Lineberger, *J. Chem. Phys.* **1992**, *96*, 8012–8020.

[10] a) J. C. Gómez Martín, O. Gálvez, M. T. Baeza-Romero, T. Ingham, J. M. C. Plane, M. A. Blitz, *Phys. Chem. Chem. Phys.* **2013**, *15*, 15612–15622; b) N. Wei, C. Hu, S. Zhou, Q. Ma, P. Mikuška, Z. Večeřa, Y. Gai, X. Lin, X. Gu, W. Zhao, B. Fang, W. Zhang, J. Chen, F. Liu, X. Shan, L. Sheng, *RSC Adv.* **2017**, *7*, 56779–56787.

[11] Z. Zhang, P. S. Monks, L. J. Stief, J. F. Liebman, R. E. Huie, S.-C. Kuo, R. B. Klemm, *J. Phys. Chem.* **1996**, *100*, 63–68.

[12] P. Hassanzadeh, K. K. Irikura, R. D. Johnson, *J. Phys. Chem. A* **1997**, *101*, 6897–6902.

[13] P. S. Monks, L. J. Stief, D. C. Tardy, J. F. Liebman, Z. Zhang, S.-C. Kuo, R. B. Klemm, *J. Phys. Chem.* **1995**, *99*, 16566–16570.

[14] a) T. Baer, B. Sztaray, J. P. Kercher, A. F. Lago, A. Bödi, C. Skull, D. Palathinkal, *Phys. Chem. Chem. Phys.* **2005**, *7*, 1507–1513; b) T. Baer, R. P. Tuckett, *Phys. Chem. Chem. Phys.* **2017**, *19*, 9698–9723.

[15] a) P. Hemberger, M. Lang, B. Noller, I. Fischer, C. Alcaraz, B. K. Cunha de Miranda, G. A. Garcia, H. Soldi-Lose, *J. Phys. Chem. A* **2011**, *115*, 2225–2230; b) G. A. Garcia, B. Gans, J. Krüger, F. Holzmeier, A. Röder, A. Lopes, C. Fittschen, C. Alcaraz, J. C. Loison, *Phys. Chem. Chem. Phys.* **2018**, *20*, 8707–8718; c) G. A. Garcia, X. Tang, J.-F. Gil, L. Nahon, M. Ward, S. Batut, C. Fittschen, C. A. Taatjes, D. L. Osborn, J.-C. Loison, *J. Chem. Phys.* **2015**, *142*, 164201; d) J. M. Dyke, *Phys. Chem. Chem. Phys.* **2019**, *21*, 9106–9136.

[16] E. Reusch, F. Holzmeier, P. Constantinidis, P. Hemberger, I. Fischer, *Angew. Chem. Int. Ed.* **2017**, *56*, 8000–8003; *Angew. Chem.* **2017**, *129*, 8113–8116.

[17] D. Schleier, A. Humeniuk, E. Reusch, F. Holzmeier, D. Nunez-Reyes, C. Alcaraz, G. A. Garcia, J. C. Loison, I. Fischer, R. Mitric, *J. Phys. Chem. Lett.* **2018**, *9*, 5921–5925.

[18] D. Schleier, P. Constantinidis, N. Faßheber, I. Fischer, G. Friedrichs, P. Hemberger, E. Reusch, B. Sztáray, K. Voronova, *Phys. Chem. Chem. Phys.* **2018**, *20*, 10721–10731.

[19] T. Bierkandt, P. Hemberger, P. Oßwald, M. Köhler, T. Kasper, *Proc. Combust. Inst.* **2017**, *36*, 1223–1232.

[20] P. Hemberger, V. B. F. Custodis, A. Bodi, T. Gerber, J. A. van Bokhoven, *Nat. Commun.* **2017**, *8*, 15946.

[21] L. Brewer, J. Tellinghuisen, *J. Chem. Phys.* **1972**, *56*, 3929–3938.

[22] J. M. Dyke, *J. Chem. Phys.* **2000**, *112*, 6262–6273.

[23] a) C. E. Miller, E. A. Cohen, *J. Chem. Phys.* **2001**, *115*, 6459–6470; b) K. A. Peterson, B. C. Shepler, D. Figgen, H. Stoll, *J. Phys. Chem. A* **2006**, *110*, 13877–13883.

[24] B. Sztaray, K. Voronova, K. G. Torma, K. J. Covert, A. Bodi, P. Hemberger, T. Gerber, D. L. Osborn, *J. Chem. Phys.* **2017**, *147*, 013944.

[25] A. Bodi, B. Sztaray, T. Baer, M. Johnson, T. Gerber, *Rev. Sci. Instrum.* **2007**, *78*, 084102.

[26] B. Sztáray, T. Baer, *Rev. Sci. Instrum.* **2003**, *74*, 3763–3768.

[27] M. J. Frisch, G. W. Trucks, H. B. Schlegel, G. E. Scuseria, M. A. Robb, J. R. Cheeseman, G. Scalmani, V. Barone, B. Mennucci, G. A. Petersson, H. Nakatsuji, M. Caricato, X. Li, H. P. Hratchian, A. F. Izmaylov, J. Bloino, G. Zheng, J. L. Sonnenberg, M. Hada, M. Ehara, K. Toyota, R. Fukuda, J. Hasegawa, M. Ishida, T. Nakajima, Y. Honda, O. Kitao, H. Nakai, T. Vreven, J. A. Montgomery, J. E. Peralta, F. Ogliaro, M. Bearpark, J. J. Heyd, E. Brothers, K. N. Kudin, V. N. Staroverov, R. Kobayashi, J. Normand, K. Raghavachari, A. Rendell, J. C. Burant, S. S. Iyengar, J. Tomasi, M. Cossi, N. Rega, J. M. Millam, M. Klene, J. E. Knox, J. B. Cross, V. Bakken, C. Adamo, J. Jaramillo, R. Gomperts, R. E. Stratmann, O. Yazyev, A. J. Austin, R. Cammi, C. Pomelli, J. W. Ochterski, R. L. Martin, K. Morokuma, V. G. Zakrzewski, G. A. Voth, P. Salvador, J. J. Dannenberg, S. Dapprich, A. D. Daniels, Farkas, J. B. Foresman, J. V. Ortiz, J. Cioslowski, D. J. Fox, Gaussian 09, Revision B.01, Gaussian Inc. Wallingford CT, **2009**.

[28] V. A. Mozhayskiy, A. I. Krylov, ezSpectrum, http://iopenshell.usc.edu/downloads **2014**.

Manuscript received: August 15, 2019
Version of record online: September 11, 2019